ACS APPLIED MATERIALS & INTERFACES

Research Article

Cite This: ACS Appl. Mater. Interfaces 2019, 11, 5561−5569

www.acsami.org

Polymeric Nanofilter Biointerface for Potentiometric Small-Biomolecule Recognition

Shoichi Nishitani and Toshiya Sakata*

Department of Materials Engineering, School of Engineering, The University of Tokyo, 7-3-1 Hongo, Bunkyo-ku, Tokyo 113-8656, Japan

Supporting Information

ABSTRACT: In this paper, we propose a novel concept of a biointerface, a polymeric nanofilter, for the potentiometric detection of small biomolecules using an extended-Au-gate field-effect transistor (EG-Au-FET). A Au electrode has the potential capability to detect various small biomolecules with ultrasensitivity at nM levels on the basis of a surface redox reaction, but it exhibits no selective response to such biomolecules. Therefore, a suitable polymeric nanofilter is designed and modified on the Au electrode, so that a small target biomolecule reaches the Au surface, resulting in an electrical signal, whereas low-molecular-weight interferences not approaching the Au surface are captured in the polymeric nanofilter. The polymeric nanofilter is composed of two layers. The first layer is electrografted as an anchor layer by a cyclic voltammetry method. Then, a filtering layer is precisely polymerized as the second layer by a photo-mediated surface-initiated atom transfer radical polymerization method. The thickness and density of the polymeric nanofilter are controlled to specifically detect a small target biomolecule with high sensitivity. As a model case, L-cysteine as the small target biomolecule at nM levels is specifically detected by filtering L-DOPA as a low-molecular-weight interference using the polymeric nanofilter-grafted EG-Au-FET on the basis of the following mechanism. The phenylboronic acid (PBA) that copolymerizes with the polymeric nanofilter captures L-DOPA through diol binding, whereas L-cysteine reaches the Au surface through the filter layer. The polymeric nanofilter can also effectively prevent the interaction between biomacromolecules such as albumin and the Au electrode. A platform based on a polymeric nanofilter-grafted EG-Au-FET biosensor is suitable for the ultrasensitive and specific detection of a small biomolecule in biological samples such as tears and sweat, which include small amounts of low-molecular-weight interferences, which generate nonspecific electrical signals.

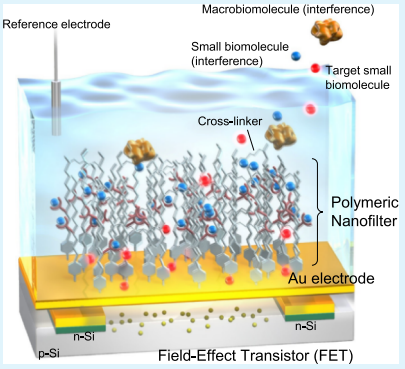

KEYWORDS: *field-effect transistor (FET), small biomolecule, polymeric nanofilter, Au electrode, specific detection*

INTRODUCTION

Small biomolecules are often recognized as significant biomarker candidates in the field of in vitro diagnostics.[1] For the detection of small biomolecules, conventional methods require enzymatic reactions and secondary antibodies with fluorescent dyes in immunoassays,[2−7] but there is a possibility that fluorescent conjugates cannot be formed in the case of smaller target biomolecules, that is, antigens.[8,9] Although enzymes and antibodies have been utilized in various scientific fields and their use has been recognized as the global standard, the use of these biomacromolecules is problematic owing to their fragility, high cost, and time-consuming production and the difficulty of quality control in their bioproduction. Therefore, an artificial and functional membrane with a standard concept should become a platform providing molecular recognition sites for small biomarkers.

Solution-gate field-effect transistors (FETs) have attracted global attention in the field of biosensor technology. Because Bergveld proposed an ion-sensitive solid-state device for neurophysiological measurements in 1970,[10] an ion-sensitive FET has been commonly used as the basic structure of ion sensors[10,11] and potentiometric biosensors,[12−18] with various semiconducting materials used as the channel, including both inorganic and organic materials.[19−24] As the gate insulator, oxide membranes such as SiO_2 and Ta_2O_5 are generally utilized owing to their pH responsivity based on the equilibrium reaction between hydrogen ions and hydroxyl groups at the gate/solution interface,[25,26] while ion-sensitive membranes or probe molecules are tethered onto gate insulators to selectively detect target ions or biomolecules.[13,15,27−30] Moreover, an Au thin film is used as the gate electrode of an extended-Au-gate field-effect transistor (EG-Au-FET), in which the gate electrode is separated and extended from the metal gate of FET (Figure 1a) because probe molecules with thiol groups are easily immobilized on the Au gate by −S−Au binding.[31−34] However, unless modified, Au exhibits a strong catalytic action, resulting in the oxidation of organic compounds, even small biomolecules such as glucose.[35−37] In addition, the Au surface is assumed to be oxidized upon exposure to UV/ozone;[38−40] therefore, the

Received: November 14, 2018
Accepted: January 15, 2019
Published: January 15, 2019

DOI: 10.1021/acsami.8b20010
ACS Appl. Mater. Interfaces 2019, 11, 5561−5569

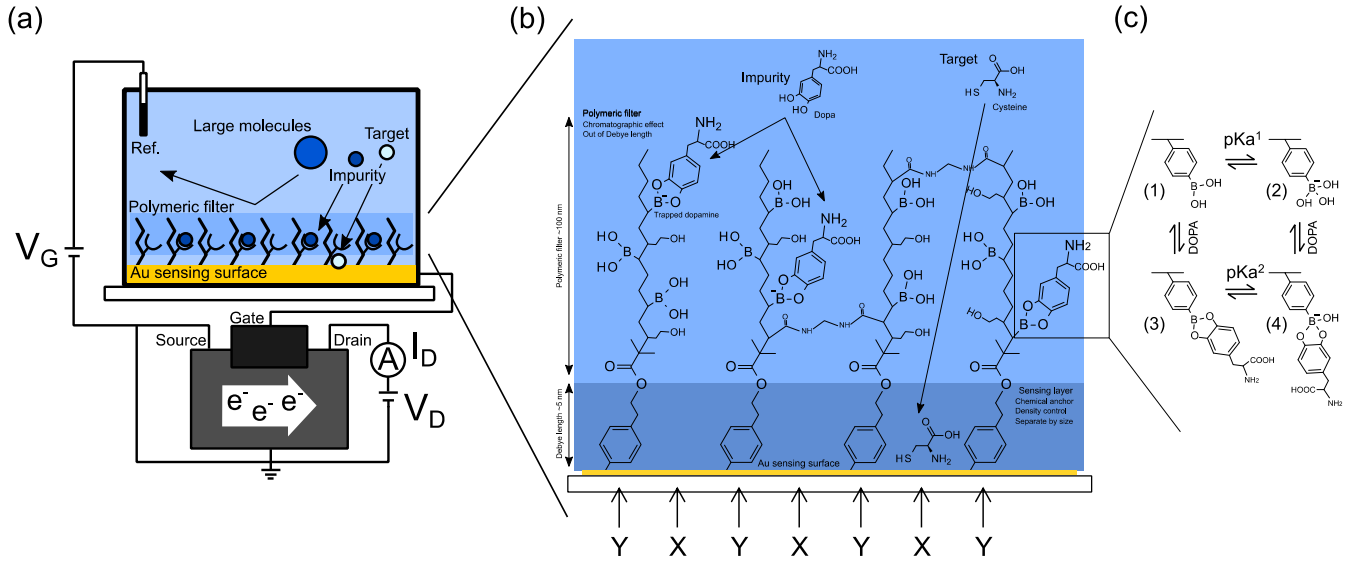

Figure 1. (a) Conceptual illustration of EG-Au-FET biosensor with nanofilter interface. (b) Conceptual design of nanofilter interface to trap L-DOPA and specifically detect cysteine by Au electrode. (c) Binding equilibrium of L-DOPA and PBA.

Scheme 1. Schematic Illustration of Surface Modification Steps[a]

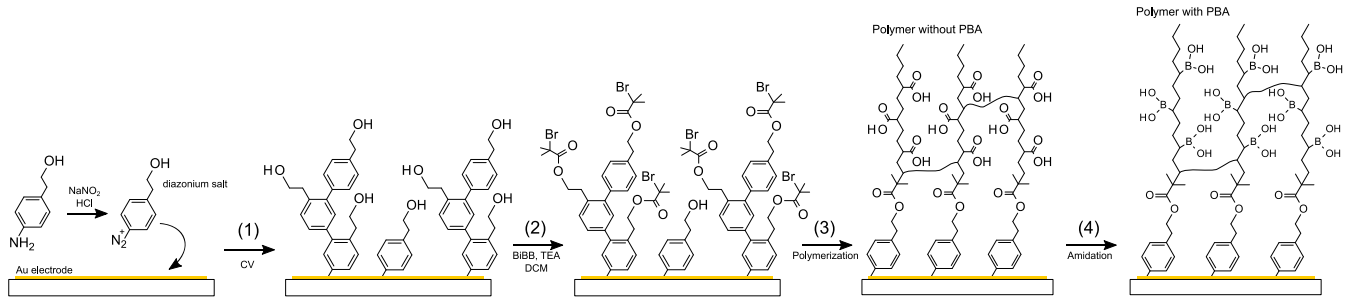

[a](1) Modification of anchor layer via cyclic voltammetry. (2) Introduction of initiator via esterification. (3) Photo-mediated SI-ATRP starting at the surface. (4) Introduction of PBA via amidation.

oxidized surface is easily reduced by the surface redox reaction with small biomolecules (see Figure S1). As a result, an electromotive force is generated at an Au film on the basis of the Nernstian equation.[41] That is, an Au electrode is very useful for the highly sensitive detection of small organic biomolecules but without detection specificity (see Figure S2). That is, when the sensor surface is well designed, where only a small target biomolecule reaches and interacts with the sensing Au surface, then specific detection can be realized. Following this strategy, a polymeric nanofilter interface is designed and synthesized on the Au surface (Figure 1b), where low-molecular-weight interferences are captured so that they cannot reach the Au surface, whereas small target biomolecules penetrate into the nanofilter membrane and reach and react with the Au surface by redox, resulting in electrical signal generation. In this case, the thickness of the filter membrane should be controlled to the order of nm so as not to reduce the speed of the response to a small target biomolecule interacting with the Au surface. On the other hand, the use of a membrane with a porous morphology for filtering biomolecules has been considered in size-exclusion-based separation techniques,[42] and a previous work showed that the inherent filtering capability and unique signal generation properties of porous silicon devices can be exploited in optical biosensing by the size-based exclusion of cells and proteins larger than the pores from interacting with the transducer surface.[43] However, our strategy realizes the specific detection of a small target biomolecule in a sample solution including not only biomacromolecules such as proteins but also low-molecular-weight interferences on the basis of the potentiometric method.

In this paper, we propose a novel concept of chemical modification. Namely, a polymeric nanofilter is used to modify an Au electrode surface. In particular, we demonstrate the effect of the polymeric nanofilter interface on the highly sensitive and specific detection of a small biomolecule for two different amino acids of L-cysteine (MW, 121) and L-DOPA (MW, 197) using the EG-Au-FET, as a model case.

RESULTS AND DISCUSSION

Concept of Polymeric Nanofilter Biointerface. The design of the polymeric nanofilter interface on the gate electrode of the EG-Au-FET is shown in Figure 1b. The interface is composed of two layers: an anchor layer and a filter layer. The anchor layer, shown in dark blue, is tethered to the Au-sensing surface under the filter layer, which determines the gap of the sensing capability at the Au substrate (X) as well as the density of the polymeric nanofilter (Y). The filter layer, shown in light blue, provides the chromatographic effect, in which low-molecular-weight interferences are captured and

DOI: 10.1021/acsami.8b20010
ACS Appl. Mater. Interfaces 2019, 11, 5561−5569

through which only a small target biomarker reaches the Au-sensing surface. Because potentiometric biosensors can detect changes in surface charges within the diffusion layer with a few nanometers from the sensing surface,[44−47] which is known as the Debye length,[48] the filter layer is located at a distance further than the Debye length. Consequently, the electrical noise caused by the binding events in the filter layer can be eliminated. As a model case to clarify the detection principle, in this study, the polymeric nanofilter biointerface was designed to detect of L-cysteine as the small target biomolecule on the Au-sensing surface and to capture L-DOPA as a low-molecular-weight interference in the filter layer.

The anchor layer was formed using a diazonium salt. Surface modification using diazonium salts has been attracting much attention owing to their high chemical stability, ease of functionalization, and the flexibility of surface design.[49] The modification involves steps (1) and (2) in Scheme 1. When a reductive potential is applied at the electrode surface in the presence of an aryldiazonium salt, the diazonium molecule is reduced to its corresponding radical. The produced radicals immediately react with the electrode surface to form a stable film via covalent bonding. The covalently bonded film is chemically stable and can tolerate UV irradiation.[50] In addition, a multilayer film with a thickness of a few nanometers is formed by chain reactions between benzene rings at the diazonium film tethered onto the Au electrode and unreacted radicals (step (1)). Multilayer film formation provides a significant advantage in developing the nanofilter interface because it enables the control of the thickness of the anchor layer to approximately the same as the Debye length. The functionality of the film can be freely designed by modifying the molecular structure of the aryldiazonium salt. In this study, the aryldiazonium salt, which was a hydroxyl group at the para-substituent of the benzene ring, was first utilized to develop the multilayer film. Then, the surface was further functionalized by introducing the initiator of the surface-initiated atom transfer radical polymerization (SI-ATRP) of the polymeric filter via esterification reactions [step (2)].

To design a filter layer that captures L-DOPA but not L-cysteine, phenylboronic acid (PBA) was included in the filter layer. PBA can form stable esters with diol-containing molecules such as L-DOPA via the equilibrium shown in Figure 1c.[51] In general, the diol binding to boronic acid decreases the pK_a of boron-containing functional groups.[52,53] Because boronic acid is a Lewis acid, it can react with a water molecule and change from the neutral trigonal form (1) to the anionic tetrahedral form (2), as shown in Figure 1c. The same reaction also occurs for the diol−boronic complex or boronate ester (3), which reacts with a water molecule to become anionic (4). As mentioned above, the pK_a of the boronate ester (pK_a^2) is lower than that of boronic acid (pK_a^1), and the density of negative charges increases proportionally to the concentration of diols. As shown in a previous work,[53] the association constant of catechol was 830 M^{-1} higher than that of other diol compounds at pH 7.4; thus, L-DOPA should have a high affinity for PBA at pH 7.4 in this study. That is, L-DOPA is captured by the PBA-containing filter layer, whereas L-cysteine is expected to reach the Au-sensing surface. In addition, PBA has the anionic form when it binds to L-DOPA (Figure 1c). As a result, the potential may change in the filter layer, but the filter layer is located outside the detection range (Debye length) of the potentiometric sensor; thus, no such electrical noise is detected. To investigate the filtering capability of the polymeric nanofilter, two types of polymeric nanofilter were designed, namely, with and without PBA. First, a methacrylic acid (MAA)-based polymer (control nanofilter) was designed (step (3) in Scheme 1) and then PBA was introduced into the filter via amidation reactions (PBA-containing nanofilter) (step (4) in Scheme 1). To control the factors of the nanofilter other than the presence or absence of PBA, such as its thickness and composition, a photo-mediated SI-ATRP method was employed in this study because the conventional ATRP method is incompatible with MAA polymerization, whereas the photo-mediated SI-ATRP method was reported to be tolerant to MAA polymerization.[54] Moreover, as shown in Figure S3, 2-hydroxyethyl methacrylate (HEMA) was utilized to make the polymer hydrophilic. Controlling the hydrophilicity is an important factor because the small target biomolecule must reach the Au electrode surface through the nanofilter. Finally, the filter layer was cross-linked to form a rigid polymer structure using a hydrophilic cross-linker, *N*,*N*′-methylenebisacrylamide (MBAAm). This is because the absence of cross-linking may generate electrical noise arising from changes in the polymer conformation induced by the binding of low-molecular-weight interferences with PBA in the nanofilter. In fact, the change in the capacitance (ΔC) of the glucose-templated molecularly imprinted polymers (MIPs) was small at various glucose concentrations in a previous study.[55] In ref 55, the MIP hydrogel included HEMA as the main chain monomer, similar to in this study, which is a hydrophilic polymer even before adding glucose. Also, the cross-link density in the glucose-templated MIP was relatively high. Thus, the rate of swelling of the glucose-templated MIP hydrogel was relatively low owing to its intrinsic hydrophilicity and relatively high cross-link density, resulting in no electrical noise in, for example, ΔC.

Surface Modification and Characterization. In the first step of surface functionalization, the anchor layer was grafted on an Au electrode by the electrochemical reduction of phenethyl ethanol (PE) diazonium salt. A cyclic voltammogram of the electrochemical grafting of PE is shown in Figure 2a. The single current peak observed in the first cycle at approximately 0 V reveals the occurrence of an irreversible reduction around the Au electrode, indicating successful grafting.[56] The peak current decreased gradually in the next few cycles and completely disappeared after five cycles, when the surface grafting reached the maximum; that is, the grafted nanolayer acted as an insulator to limit further grafting processes. Additionally, the grafting was confirmed by the change in the surface hydrophilicity. As shown in Figure 2b, the electrochemically modified Au surface became significantly hydrophilic after the modification of PE with five cycles [see the contact angles (CAs) on the Au and OH surfaces shown in the figure] because the Au electrode surface was covered by hydroxyl groups based on PE.

To characterize the electrochemically grafted surface after five cycles, the graft density was calculated from the reductive current shown in Figure 2a, assuming a one-electron reaction. The number of grafted PE molecules after five cycles per square nanometer was 49.5 ± 2.4, which indicates the formation of a multilayer film (step (1) in Scheme 1). In addition, the thickness of the grafted PE film after five cycles was 6.2 ± 2.4 nm and the surface roughness (R_q) of the unmodified Au and PE-grafted Au was in the range from 1 to 2 nm, but the surface morphology of the PE-grafted Au showed smaller irregularities than that of the unmodified Au, which

DOI: 10.1021/acsami.8b20010
ACS Appl. Mater. Interfaces 2019, 11, 5561−5569

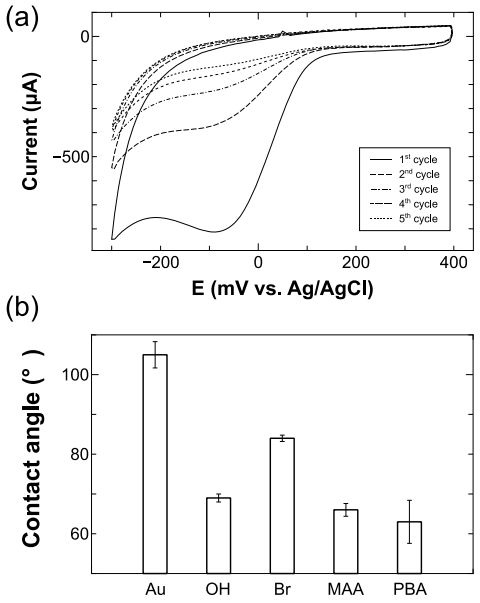

Figure 2. (a) Cyclic voltammogram of electrochemical grafting of PE diazonium salt on Au electrode. The sweeps were consecutively recorded in five cycles in 2 mM DSOH in 0.5 M HCl from 0.4 V to −0.3 V at 50 mV/s. (b) Wettability profile of the following samples from the left: bare Au electrode, PE-modified Au electrode, alkyl bromide Au electrode, co-(MAA)−(HEMA)−(MBAAm) polymerized on Au electrode, and the polymer with PBA on Au electrode.

were estimated by atomic force microscopy (AFM) (see Figure S4). Considering the immobilization density and thickness of PE layer, the gap between PE molecules at the Au surface was calculated to be about 0.5 nm (see Figure S5), which is sufficiently large to allow small biomolecules such as L-cysteine and ascorbic acid (AA) to come in contact with the Au surface. As mentioned in the previous section, controlling the thickness of the anchor layer is important in minimizing the electrical noise generated by interferences in a sample solution. If the filter layer is partially located inside the Debye diffusion layer at the electrolyte/Au electrode interface, low-molecular-weight interferences binding to the filter may contribute to electrical noise. In this study, negative charges based on the L-DOPA−PBA binding may generate critical noise. Considering that the Debye length at the solution/Au electrode interface in 10 mM phosphate buffer solution is approximately 3 nm, which was calculated using an equation introduced in previous works,[44−47] the thickness of the anchor layer (see Figure S4) was greater than the Debye length. Moreover, as shown in Figure S6, the anchor layer electrografted after five cycles allowed a small molecule, ascorbic acid (MW 176) to reach the Au surface because gaps remained between the PE molecules at the Au surface; as shown in Figure 1b, the sensing capability depended on the gap length at the Au substrate (X). However, the anchor layer prevented biomacromolecules such as bovine serum albumin (MW ca. 66 kDa), human serum albumin (HSA: MW ca. 66 kDa), and amylase (MW ca. 54−62 kDa) from interacting with the Au surface. Moreover, the highly sensitive detection of AA as a small biomolecule was found using the EG-Au-FET with the anchor layer, even when HSA (0.3 mg/mL) was included in the sample solution. Thus, the anchor layer electrografted on the Au electrode was satisfactory in terms of the thickness and density of PE for the purpose of this study.

After introducing the ATRP initiator 2-bromoisobutyryl bromide (BiBB) onto the anchor layer, the photo-mediated SI-ATRP was conducted to form the filter layer. The successful introduction of the ATRP initiator was confirmed by CA measurement. Figure 2b shows that the surface became more hydrophobic after the introduction of the ATRP initiator because the ATRP initiator contained a bromo group. Prior to the surface modification based on the photo-mediated SI-ATRP, the polymerization conditions were investigated. As shown in Figure S7, a copolymer gel was formed only when both the initiator ethyl 2-bromoisobutyrate (EBiB) and the catalyst [fac-Ir(ppy)$_3$] were used during UV irradiation in the polymerization process. When one of the reagents was not included in the solution, no polymerization occurred. Moreover, photo-mediated SI-ATRP was time-dependent, indicating the successful control of the polymerization (see Figure S7). One of the reasons why we used the photo-mediated SI-ATRP method was its compatibility with MAA, the main monomer used in the filter layer. In typical ATRP, acidic monomers such as MAA prevent the propagation of polymerization.[50,54] On the other hand, the use of the photo-mediated SI-ATRP method leads to successful polymerization. In this case, the thickness of the polymeric nanofilter was assumed to be in the range of 100−150 nm on the basis of the 24 h duration of photo-mediated SI-ATRP in this study as the rate of increase in the thickness was approximately 6 nm/h in a previous paper.[50] As shown in Figure 2b, the surface became hydrophilic after the photo-mediated SI-ATRP because the polymer contains carboxyl groups. The introduction of PBA did not affect the wettability of the polymer, probably because of excess MAA in the polymer.

Real-Time Monitoring of Changes in Concentrations of L-cysteine and L-DOPA Using EG-Au-FET. First, the detection sensitivity of the sensor without the polymeric nanofilter was investigated using the EG-Au-FET, as shown in Figure 3. In this sensor, an unmodified Au electrode was

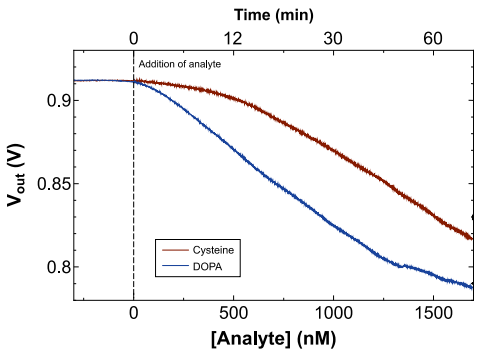

Figure 3. Real-time change in surface potential following the addition of cysteine (black line) and L-DOPA (blue line) measured using EG-Au-FET system. Both analytes were injected at a concentration of 0.03 mM and a rate of 5 μL/min. The top axis shows the corresponding time in minutes (analyte solution was injected starting at 0 min).

simply connected to the gate of the FET. L-cystine and L-DOPA were separately injected into the sensor system using a syringe pump, and the change in surface potential was monitored in real time. Upon the initial injection of analyte L-cystine and L-DOPA solutions at 0 min (see the top axis in Figure 3), the surface potentials immediately shifted in the negative direction, and continually decreased with increasing

DOI: 10.1021/acsami.8b20010
ACS Appl. Mater. Interfaces 2019, 11, 5561−5569

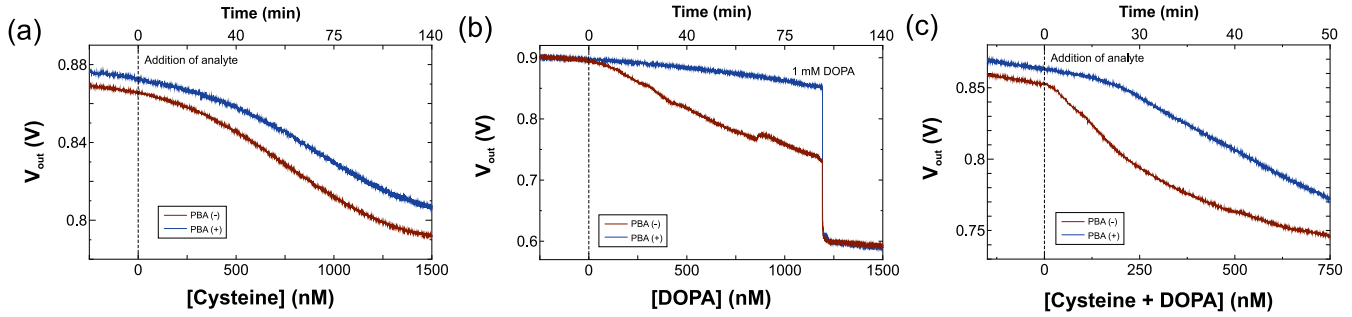

Figure 4. Changes in surface potential for the continuous addition of analytes to the Au-FET biosensors with the surface modified by polymer with (blue line) or without (red line) PBA. The top axis shows the time in min, corresponding to the concentration of analyte. The injection of analyte started at 0 min. (a) Addition of 0.03 mM L-cysteine at 5 μL/min. (b) Addition of 0.03 mM L-DOPA at 5 μL/min. (c) Addition of mixture of 0.03 mM L-DOPA and 0.03 mM L-cysteine at 5 μL/min.

analyte concentration in the sensor. The x-axis was converted to the concentration of the analytes using eq 2 (see Methods), and then the detection sensitivity for both analytes was determined to be on nM order.

The highly sensitive detection by the EG-Au-FET sensor was due to the oxidative property of the Au electrode. The surface of the Au electrode is partially covered by the oxide layer formed by the oxidation.[38−40] In addition, the oxidized Au layer can be used as a catalyst for small biomolecules such as L-DOPA (see Figure S1). As previously reported, the oxidized Au surface is assumed to consist of Au(3), and the oxidation of small biomolecules occurs when Au(3) is reduced to Au(0). Therefore, the detection mechanism of the EG-Au-FET can be simplified to that shown in Figure S1. On the basis of the surface redox reaction with L-DOPA, the Au surface becomes slightly electron-rich, which was detected as the change in the surface potential using the EG-Au-FET sensor. On the other hand, alkanethiol covalently binds to Au, resulting in functional membrane formation at the gate surface, as represented by[57−61]

$$\mathrm{R{-}SH + Au \rightarrow R{-}S{-}Au + H^{+} + e^{-}} \quad (1)$$

Thus, the Au surface also becomes slightly electron-rich following its reaction with L-cysteine. This is the reason why the interaction between L-cysteine and the Au electrode was detected as a change in surface potential using the EG-Au-FET sensor.

Effect of Polymeric Nanofilter on Electrical Noises Based on Low-Molecular-Weight Interference. The chromatographic effect of the polymeric nanofilter was investigated by adding analytes to the EG-Au-FET coated with the polymeric nanofilter with or without PBA, namely, the PBA−FET or the non-PBA−FET. Figure 4a shows the change in surface potential for the continuous injection of L-cysteine. As expected from the design of the polymeric nanofilter, the target model L-cysteine was similarly detected in both sensors. This result was also supported by the calibration curve obtained from Figure 4a (see Figure S8A). Because L-cysteine did not bind to PBA in the polymeric nanofilter, it could reach the Au-sensing surface, regardless of the presence or absence of PBA in the nanofilter. The diffusion of target small biomolecules in the polymeric nanofilter may depend on the density of the cross-linker copolymerized in it, but the filter layer did not prevent the diffusion of L-cysteine under the condition used in this study. Then, the interference model L-DOPA was measured using both sensors. As shown in Figure 4b, the detection sensitivities were clearly different between the PBA−FET and non-PBA−FET sensors, which was supported by the calibration curve obtained from Figure 4b (see Figure S8B). The PBA−FET sensor (blue line) showed a significantly lower detection sensitivity than the non-PBA−FET sensor because L-DOPA was trapped by PBA in the nanofilter and did not reach the Au sensing surface. Thus, the effect of the polymeric nanofilter was clearly demonstrated as expected. Then, the nonspecific signal based on L-DOPA as a small interference molecule was found to be suppressed to about 73% by the polymeric nanofilter with PBA, which was calculated from the relative change (P %) in the electrical signal using the PBA−FET from that using the non-PBA−FET at 1 μM of L-DOPA [(100 − P)%]. On the basis of this estimation, we further investigated the repeatability and reproducibility of the proposed sensors by analyzing the effect of the polymeric nanofilter on the prevention of nonspecific signals. As a result, we obtained a suppression of 72.7 ± 12.6% (N = 6), which shows good reproducibility. When the concentration of L-DOPA was also increased to 1 mM, the surface potentials for both sensors dropped to the same value. This indicates that the nanofilter has a certain capacity that depends on the amount of PBA in the nanofilter. Finally, the sensor specificity was investigated by adding a mixture of L-cysteine and L-DOPA. In Figure 4c, the PBA−FET (blue line) clearly showed a change in surface potential after adding the mixed solution but had a smaller response than the non-PBA−FET (red line). On the other hand, the non-PBA−FET sensor should have responded to both analytes owing to its nonfiltering effect, resulting in a stronger signal. Considering Figure 4a,b, the difference in the intensity of electrical signals between the PBA−FET and non-PBA−FET sensors shown in Figure 4c (also see Figure S8C) should be based on the prevention of L-DOPA from approaching the Au surface. Therefore, L-DOPA was successfully trapped by the nanofilter, whereas L-cysteine was specifically detected at nM levels using the PBA−FET sensor. However, the detection sensitivities appeared to be similar for the PBA−FET and non-PBA−FET sensors in the mixture (see Figure S8C). This may be because there is an interaction between each analyte in the mixture. The suppressing effect of the polymeric nanofilter on the nonspecific signals based on L-DOPA (a small interference biomolecule) also appeared to be reduced at higher concentrations of the mixture; thus, the amount of PBA in the polymeric nanofilter will be strictly controlled depending on the target biomolecule in the future.

Moreover, the reaction rates for L-cysteine and L-DOPA interacting with the Au electrode were estimated using the EG-

DOI: 10.1021/acsami.8b20010
ACS Appl. Mater. Interfaces 2019, 11, 5561−5569

Au-FET with or without the polymeric filter. Figure 5 shows the change in the surface potential per reaction time for

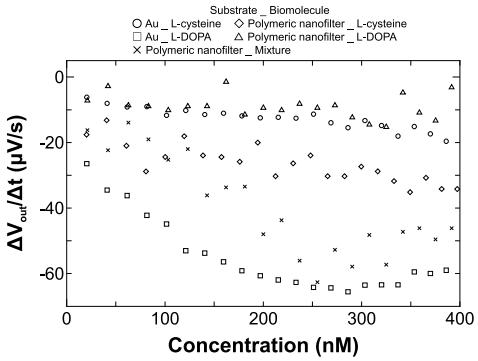

Figure 5. Reaction rates for L-cysteine and L-DOPA interacting with the Au electrode using the EG-Au-FET with or without the polymeric filter. These reaction rates were calculated on the basis of the data obtained in Figures 3 and 4. L-Cysteine was added onto the unmodified Au electrode (○) or the polymeric nanofilter-coated Au electrode (◇), L-DOPA was added onto the unmodified Au electrode (□) or the polymeric nanofilter-coated Au electrode (△), and their mixture was added onto the polymeric nanofilter-coated Au electrode (×). In this figure, all the polymeric nanofilters contained PBA receptors.

different concentrations of each analyte. These reaction rates were calculated on the basis of the data obtained in Figures 3 and 4; that is, the surface potential (V_{out}) was averaged over every 10 s and the reaction rates (μV/s) were calculated as the change in the average V_{out} (ΔV_{out}) per 10 s. For the cases in Figures 3 and 4, each analyte was injected with a concentration of 0.03 mM at a rate of 5 μL/min using a syringe pump. As a result, the concentration of the analytes continuously and gradually increased with time, which was directly converted to the analyte concentration using eq 2 (see Methods). As shown in Figure 5, the reaction rate for L-DOPA interacting with the Au electrode was clearly decreased by the polymeric filter (see □ and △ plotted in Figure 5) owing to the PBA/L-DOPA diol binding inside the polymeric filter but outside the diffusion layer at the solution/Au interface. In contract, the reaction rate for L-cysteine interacting with the Au electrode was maintained despite the coating of the polymeric filter on the Au gate (see ○ and ◇ plotted in Figure 5). Furthermore, the reaction rate for the mixture of L-cysteine and L-DOPA interacting with the Au electrode (see × plotted in Figure 5) was similar to that for L-cysteine (see ○ and ◇ plotted in Figure 5) below a concentration of about 250 nM for each analyte in the mixture. This means that L-cysteine was specifically detected by the prevention of L-DOPA from interacting with the Au electrode using the polymeric nanofilter-grafted EG-Au-FET. However, the reaction rate for the mixture above a concentration of about 250 nM (see × plotted in Figure 5) seemed to approach that for L-DOPA detected using the EG-Au-FET without the polymeric filter (see □ plotted in Figure 5). That is, in future, the amount of PBA in the polymeric nanofilter should be controlled to capture more interferences at higher concentrations. Thus, we have clarified the concept of a polymeric nanofilter biointerface for use as a potentiometric biosensor to specifically detect a small target biomolecule at nM levels in this study.

CONCLUSION

To utilize the characteristics of a potentiometric EG-Au-FET biosensor, we have presented a polymeric nanofilter as a novel concept of a biointerface for the ultrasensitive and specific detection of small biomolecules. First, an anchor layer was grafted as the first layer on the Au electrode by the electrochemical reduction of a PE diazonium salt. Then, the filtering layer with PBA, which functioned as the receptor molecule for a small interference biomolecule, was precisely polymerized as the second layer by the photo-mediated SI-ATRP method, which enabled the thickness and density of the polymeric nanofilter to be controlled to specifically detect a small target biomolecule. As a model case, L-DOPA was successfully trapped by the nanofilter, whereas L-cysteine was specifically detected at nM levels using the polymeric-nanofilter-coated EG-Au-FET with PBA. The polymeric nanofilter also effectively prevented the interaction between a few biomacromolecules and the Au electrode. Thus, we have proved the concept of the polymeric nanofilter for the specific detection of small biomolecules using the EG-Au-FET biosensor, which will be applied for various small biomarkers to modify the nanofilter composition.

METHODS

Materials. 2-(4-Aminophenyl)ethanol (APE), BiBB, and EBiB were purchased from Tokyo Chemical Industry. Tetrafluoroboric acid (HBF_4), sodium nitrite ($NaNO_2$), triethylamine (TEA), MAA, HEMA, MBAAm, tris(2-phenylpyridinato)iridium(III) (fac-Ir(ppy)$_3$), 4-(4,6-dimethoxy-1,3,5-triazin-2-yl)-4-methylmorpholinium chloride, *m*-aminoPBA, dopamine hydrochloride, 3-(3,4-dihydroxyphenyl)-L-alanine (L-DOPA), L-cysteine, *N*,*N*-dimethylformamide, 1 M HCl, dichloromethane, solid NaCl, Na_2HPO_4, NaH_2PO_4, distilled water, ethanol, and methanol were purchased from Wako Pure Chemical Industry.

Electrochemical Grafting. A potentiostat/galvanostat (PS-14, Toho Technical Research) and a function generator (AFG3102C, Tektronix) were used for the electrochemical grafting of the anchor layer. Cyclic voltammetry (CV) was performed at 25 °C by applying a constant potential (0 V vs Ag/AgCl) using a PS-14 potentiostat/galvanostat while controlling the potential using a function generator (AFG3102C, Tektronix). The Ag/AgCl electrode was immersed in saturated KCl solution. Before the potential application, the Au electrode was cleaned by 10 min sonication in acetone, 10 min sonication in methanol, and 5 min sonication in distilled water. APE was electrochemically grafted as follows. A 100 mL solution of 0.5 M HCl was stirred in a 300 mL beaker in an ice-cold water bath. APE [28 mg (0.2 mmol)] was added to the solution, which was stirred for 5 min. Then, 1 mL of 200 mM $NaNO_2$ in water was added dropwise to the mixture, which was stirred for 15 min. A cleaned Au electrode was immersed in the mixed solution and CV was conducted in the potential range from 0.4 V to −0.3 V at 50 mV/s. After five cycles, the substrate was washed thoroughly with methanol and then with distilled water.

Surface Modification of Polymeric Nanofilter Interface on the Au Electrode. After APE was grafted on the Au electrode via the electrochemical reduction of an aryldiazonium salt,[62] APE was modified using an ATRP initiator through esterification.[63] The previously modified film was immersed in 50 mL of dichloromethane in a separate flask and stirred in ice-cold water. After adding 712 μL (5 mmol) of TEA, 628 μL (5 mmol) of 2-BiBB was added dropwise to the mixture. The mixture was stirred for 2 h below 4 °C then at r.t. for 24 h. The substrate was washed thoroughly with methanol and then with water after the modification.

The photo-mediated SI-ATRP of the surface was initiated as follows. MAA [3 mL (35 mmol)] and HEMA [1.9 mL (15 mmol)] were dissolved in 45 mL of methanol. The mixture was deoxygenated by flowing N_2 gas for 30 min. Then, the Br-modified Au substrate was

DOI: 10.1021/acsami.8b20010
ACS Appl. Mater. Interfaces 2019, 11, 5561−5569

immersed in the mixture in a separate flask while stirring with a magnet stirrer. Then, 0.69 mg of fac-Ir(ppy)$_3$ was added to the mixture. UV light was irradiated on the mixture for 24 h at 25 °C. After the polymerization, the substrate was immersed in methanol for 1 h then washed thoroughly with distilled water.

FET Real-Time Measurement. A modified or unmodified Au electrode was connected to the extended gate of a silicon-based n-channel junction-type FET (K246-Y9A, Toshiba), and gate voltage was applied through the Ag/AgCl reference electrode. The gate surface potential (V_{out}) was measured in real time using an FET real-time monitoring system (Optogenesys). In this study, constant-charge mode operation was used for all the measurements, where the gate voltage (V_G), drain voltage (V_D), and drain-source current (I_{DS}) were set to constant values and the change in V_{out} (ΔV_{out}) at the gate was measured using the source follower circuit (see Figure S9). Thus, V_{out} is a measure of the changes in surface potential or threshold voltage.

In the measurement, the sensing surface was covered with 300 μL of diluted buffer solution (10 mM phosphate buffer, pH 7.4). ΔV_{out} was monitored by applying I_{DS} = 700 μA and V_G = 0 V. After the surface potential stabilized, 0.03 mM target solution (L-DOPA or L-cysteine) was continuously injected at a constant rate (5 μL/min) using a syringe pump (Harvard) so that the concentration of the analyte continuously and gradually increased. In the analysis, time was directly converted to the analyte concentration using the following relationship (see S8)

$$C_t = \frac{M}{1 + 60V_1/kt_1} \quad (2)$$

where k is the rate of injection, V_1 (μL) is the initial volume, M (mol/L) is the concentration of injected target solution, and C_t (mol/L) is the concentration at time t_1 (s).

Surface Characterization. The sensor surface was characterized by CA measurement and AFM. A CA-W system (Kyowa Interface Science Co., Ltd.) was used for all water CA measurements in the dry state. The size of water droplets was controlled using a syringe pump. The CA was automatically estimated using the analysis software. The film thickness was measured by AFM (Agilent 5500, Toyo Corporation). The anchor layer thickness was determined by subtracting the thickness of Au over the glass plate from the thickness of the thin-film-modified Au over glass. To achieve a sharp image, the Au layer was patterned by photolithography before the Au-on-Ti sputtering process. Briefly, a positive resist (OFPR-800LB) was coated on a cleaned glass plate by spin coating (500 rpm for 5 s, followed by 3000 rpm for 30 s). The resist was prebaked at 110 °C for 3 min in a baker. Then, the plates were exposed to UV through a Cr-patterned glass mask using a high-resolution mask aligner (Q-2001CT, Quintel). The sample was immersed in a developer (NMD-W) for 12 s then rinsed using distilled water. The substrate was postbaked at 120 °C for 3 min on the baker. After sputtering Au/Ti, the samples were immersed in acetone for 1 day to extract the resist. For AFM measurement, a PPR-NCHR-10 probe (NANOSENSORS) was used. The image was analyzed using SPIP software (Image Metrology).

■ ASSOCIATED CONTENT

Supporting Information

The Supporting Information is available free of charge on the ACS Publications website at DOI: 10.1021/acsami.8b20010.

Schematic illustration of redox reaction between small biomolecules and Au surface; detection of various small biomolecules using EG-Au-FET biosensor; composition of polymeric nanofilter; evaluation of thickness of anchor layer by AFM; calculation of gap between PE molecules; suppression of electrical signal based on biomacromolecule; characterization of photo-mediated ATRP; calibration curve for EG-Au-FET coated with the polymeric nanofilter; and source follower circuit for real-time FET measurement system (PDF)

■ AUTHOR INFORMATION

Corresponding Author

*E-mail: sakata@biofet.t.u-tokyo.ac.jp. Phone: +81-3-5841-1842. Fax: +81-3-5841-1842.

ORCID

Toshiya Sakata: 0000-0003-1246-5000

Notes

The authors declare no competing financial interest.

■ ACKNOWLEDGMENTS

This study was partly supported by the Mirai program of Japan Science and Technology (JST).

■ REFERENCES

(1) Updike, S. J.; Hicks, G. P. The Enzyme Electrode. *Nature* **1967**, *214*, 986−988.

(2) Coons, A. H.; Creech, H. J.; Jones, R. N.; Berliner, E. The Demonstration of Pneumococcal Antigen in Tissues by The Use of Fluorescent Antibody. *J. Immunol.* **1942**, *45*, 159−170.

(3) Engvall, E.; Perlmann, P. Enzyme-Linked Immunosorbent Assay (ELISA). Quantitative Assay of Immunoglobulin G. *Immunochemistry* **1971**, *8*, 871−874.

(4) Suckling, C. J. Immobilized Enzymes. *Chem. Soc. Rev.* **1977**, *6*, 215−233.

(5) Palomäki, P. Simultaneous Use of Poly- and Monoclonal Antibodies as Enzyme Tracers in A One-step Enzyme Immunoassay for The Detection of Hepatitis B Surface Antigen. *J. Immunol. Methods* **1991**, *145*, 55−63.

(6) Rao, P. N.; Taraporewala, I. B. A Sensitive Enzyme-Linked Immunosorbent Assay (ELISA) for Testosterone: Use of A Novel Heterologous Hapten Conjugated to Penicillinase. *Steroids* **1992**, *57*, 154−161.

(7) Newman, J. D.; Turner, A. P. F. Home Blood Glucose Biosensors: A Commercial Perspective. *Biosens. Bioelectron.* **2005**, *20*, 2435−2453.

(8) Ueda, H.; Tsumoto, K.; Kubota, K.; Suzuki, E.; Nagamune, T.; Nishimura, H.; Schueler, P. A.; Winter, G.; Kumagai, I.; Mahoney, W. C. Open Sandwich ELISA: A Novel Immunoassay Based on The Interchain Interaction of Antibody Variable Region. *Nat. Biotechnol.* **1996**, *14*, 1714−1718.

(9) Suzuki, C.; Ueda, H.; Mahoney, W.; Nagamune, T. Open Sandwich Enzyme-Linked Immunosorbent Assay for The Quantitation of Small Haptens. *Anal. Biochem.* **2000**, *286*, 238−246.

(10) Bergveld, P. Development of An Ion-Sensitive Solid-State Device for Neurophysiological Measurements. *IEEE Trans. Biomed. Eng.* **1970**, *BME-17*, 70−71.

(11) Esashi, M.; Matsuo, T. Integrated Micro Multi Ion Sensor Using Field Effect of Semiconductor. *IEEE Trans. Biomed. Eng.* **1978**, *BME-25*, 184−192.

(12) Fromherz, P.; Offenhausser, A.; Vetter, T.; Weis, J. A Neuron-Silicon Junction: A Retzius Cell of The Leech on An Insulated-Gate Field-Effect Transistor. *Science* **1991**, *252*, 1290−1293.

(13) Sakata, T.; Miyahara, Y. DNA Sequencing Based on Intrinsic Molecular Charges. *Angew. Chem., Int. Ed.* **2006**, *45*, 2225−2228.

(14) Sakata, T.; Miyahara, Y. Noninvasive Monitoring of Transporter−Substrate Interaction at Cell Membrane. *Anal. Chem.* **2008**, *80*, 1493−1496.

(15) Sakata, T.; Ihara, M.; Makino, I.; Miyahara, Y.; Ueda, H. Open Sandwich-Based Immuno-Transistor for Label-Free and Noncompetitive Detection of Low Molecular Weight Antigen. *Anal. Chem.* **2009**, *81*, 7532−7537.

(16) Rothberg, J. M.; Hinz, W.; Rearick, T. M.; Schultz, J.; Mileski, W.; Davey, M.; Leamon, J. H.; Johnson, K.; Milgrew, M. J.; Edwards,

DOI: 10.1021/acsami.8b20010
ACS Appl. Mater. Interfaces 2019, 11, 5561−5569

M.; Hoon, J.; Simons, J. F.; Marran, D.; Myers, J. W.; Davidson, J. F.; Branting, A.; Nobile, J. R.; Puc, B. P.; Light, D.; Clark, T. A.; Huber, M.; Branciforte, J. T.; Stoner, I. B.; Cawley, S. E.; Lyons, M.; Fu, Y.; Homer, N.; Sedova, M.; Miao, X.; Reed, B.; Sabina, J.; Feierstein, E.; Schorn, M.; Alanjary, M.; Dimalanta, E.; Dressman, D.; Kasinskas, R.; Sokolsky, T.; Fidanza, J. A.; Namsaraev, E.; McKernan, K. J.; Williams, A.; Roth, G. T.; Bustillo, J. An Integrated Semiconductor Device Enabling Non-Optical Genome Sequencing. *Nature* **2011**, *475*, 348−352.

(17) Sakata, T.; Saito, A.; Mizuno, J.; Sugimoto, H.; Noguchi, K.; Kikuchi, E.; Inui, H. Single Embryo-Coupled Gate Field Effect Transistor for Elective Single Embryo Transfer. *Anal. Chem.* **2013**, *85*, 6633−6638.

(18) Yang, H.; Honda, M.; Saito, A.; Kajisa, T.; Yanase, Y.; Sakata, T. Nonoptical Detection of Allergic Response with a Cell-Coupled Gate Field-Effect Transistor. *Anal. Chem.* **2017**, *89*, 12918−12923.

(19) Sarkar, D.; Liu, W.; Xie, X.; Anselmo, A. C.; Mitragotri, S.; Banerjee, K. MoS_2 Field-Effect Transistor for Next-Generation Label-Free Biosensors. *ACS Nano* **2014**, *8*, 3992−4003.

(20) Izak, T.; Sakata, T.; Miyazawa, Y.; Kajisa, T.; Kromka, A.; Rezek, B. Diamond-Coated Field-Effect Sensor for DNA Recognition — Influence of Material and Morphology. *Diamond Relat. Mater.* **2015**, *60*, 87−93.

(21) Reiner-Rozman, C.; Larisika, M.; Nowak, C.; Knoll, W. Graphene-Based Liquid-Gated Field Effect Transistor for Biosensing: Theory and Experiments. *Biosens. Bioelectron.* **2015**, *70*, 21−27.

(22) Sakata, T.; Nishimura, K.; Miyazawa, Y.; Saito, A.; Abe, H.; Kajisa, T. Ion Sensitive Transparent-Gate Transistor for Visible Cell Sensing. *Anal. Chem.* **2017**, *89*, 3901−3908.

(23) Minamiki, T.; Sasaki, Y.; Tokito, S.; Minami, T. Label-Free Direct Electrical Detection of a Histidine-Rich Protein with Sub-Femtomolar Sensitivity using an Organic Field-Effect Transistor. *ChemistryOpen* **2017**, *6*, 472−475.

(24) Tung, N. T.; Tue, P. T.; Lien, T. T. N.; Ohno, Y.; Maehashi, K.; Matsumoto, K.; Nishigaki, K.; Biyani, M.; Takamura, Y. Peptide Aptamer-Modified Single-Walled Carbon Nanotube-Based Transistors for High-Performance Biosensors. *Sci. Rep.* **2017**, *7*, 17881.

(25) Bousse, L.; Mostarshed, S.; Van Der Shoot, B.; de Rooij, N. F.; Gimmel, P.; Göpel, W. Zeta Potential Measurements of Ta_2O_5 and SiO_2 Thin Films. *J. Colloid Interface Sci.* **1991**, *147*, 22−32.

(26) Sakata, T.; Saito, A. Review—Egg Cells on a Semiconductor: Potentials in Drug Screening and Clinical Diagnostics. *ECS J. Solid State Sci. Technol.* **2018**, *7*, Q3094.

(27) Sakata, T.; Kamahori, M.; Miyahara, Y. Immobilization of Oligonucleotide Probes on Si_3N_4 Surface and Its Application to Genetic Field Effect Transistor. *Mater. Sci. Eng. Carbon* **2004**, *24*, 827−832.

(28) Han, Y.; Offenhäusser, A.; Ingebrandt, S. Detection of DNA Hybridization by a Field-Effect Transistor with Covalently Attached Catcher Molecules. *Surf. Interface Anal.* **2006**, *38*, 176−181.

(29) Nishitani, S.; Sakata, T. Potentiometric Adsorption Isotherm Analysis of a Molecularly Imprinted Polymer Interface for Small-Biomolecule Recognition. *ACS Omega* **2018**, *3*, 5382−5389.

(30) Sakata, T. [Review] In Vitro Diagnostic Device with a Bio-Coupled Gate Field-Effect. *Int. J. Autom. Technol.* **2018**, *12*, 45−51.

(31) Bain, C. D.; Whitesides, G. M. Depth Sensitivity of Wetting: Monolayers of ω-Mercapto Ethers on Gold. *Science* **1988**, *240*, 62−63.

(32) Laibinis, P. E.; Whitesides, G. M.; Allara, D. L.; Tao, Y. T.; Parikh, A. N.; Nuzzo, R. G. Comparison of the Structures and Wetting Properties of Self-Assembled Monolayers of N-alkanethiols on the Coinage Metal Surfaces, Copper, Silver, and Gold. *J. Am. Chem. Soc.* **1991**, *113*, 7152−7167.

(33) Sakata, T.; Maruyama, S.; Ueda, A.; Otsuka, H.; Miyahara, Y. Stable Immobilization of an Oligonucleotide Probe on a Gold Substrate Using Tripodal Thiol-Derivatives. *Langmuir* **2007**, *23*, 2269−2272.

(34) Kajisa, T.; Sakata, T. Characterization of Ion-Sensitive Extended-Gate Field Effect Transistor Coated with Functional Self-Assembled Monolayer. *Jpn. J. Appl. Phys.* **2015**, *54*, 04DL06.

(35) Hutchings, G. Vapor Phase Hydrochlorination of Acetylene: Correlation of Catalytic Activity of Supported Metal Chloride Catalysts. *J. Catal.* **1985**, *96*, 292−295.

(36) Hashmi, A. S. K. Homogeneous Gold Catalysis − Still Accelerating. *J. Organomet. Chem.* **2009**, *694*, 481−598.

(37) Zope, B. N.; Hibbitts, D. D.; Neurock, M.; Davis, R. J. Reactivity of the Gold/Water Interface during Selective Oxidation Catalysis. *Science* **2010**, *330*, 74−78.

(38) King, D. E. Oxidation of Gold by Ultraviolet Light and Ozone at. 25°C. *J. Vac. Sci. Technol., A* **1995**, *13*, 1247−1253.

(39) Krozer, A.; Rodahl, M. X -ray Photoemission Spectroscopy Study of UV/ozone Oxidation of Au under Ultrahigh Vacuum Conditions. *J. Vac. Sci. Technol., A* **1997**, *15*, 1704−1709.

(40) Kibis, L. S.; Stadnichenko, A. I.; Koscheev, S. V.; Zaikovskii, V. I.; Boronin, A. I. XPS Study of Nanostructured Rhodium Oxide Film Comprising Rh^{4+} Species. *J. Phys. Chem. C* **2016**, *120*, 19142−19150.

(41) Ishige, Y.; Shimoda, M.; Kamahori, M. Extended-gate FET-based Enzyme Sensor with Ferrocenyl-alkanethiol Modified Gold Sensing Electrode. *Biosens. Bioelectron.* **2009**, *24*, 1096−1102.

(42) Létant, S. E.; Hart, B. R.; van Buuren, A. W.; Terminello, L. J. Functionalized Silicon Membranes for Selective Bio-organism Capture. *Nat. Mater.* **2003**, *2*, 391−395.

(43) Bonanno, L. M.; DeLouise, L. A. Whole Blood Optical Biosensor. *Biosens. Bioelectron.* **2007**, *23*, 444−448.

(44) Pouthas, F.; Gentil, C.; Côte, D.; Bockelmann, U. DNA Detection on Transistor Arrays Following Mutation-Specific Enzymatic Amplification. *Appl. Phys. Lett.* **2004**, *84*, 1594−1596.

(45) Sakata, T.; Miyahara, Y. Direct Transduction of Primer Extension into Electrical Signal Using Genetic Field Effect Transistor. *Biosens. Bioelectron.* **2007**, *22*, 1311−1316.

(46) Stern, E.; Wagner, R.; Sigworth, F. J.; Breaker, R.; Fahmy, T. M.; Reed, M. A. Importance of the Debye Screening Length on Nanowire Field Effect Transistor Sensors. *Nano Lett.* **2007**, *7*, 3405−3409.

(47) Palazzo, G.; De Tullio, D.; Magliulo, M.; Mallardi, A.; Intranuovo, F.; Mulla, M. Y.; Favia, P.; Vikholm-Lundin, I.; Torsi, L. Detection Beyond Debye's Length with an Electrolyte-Gated Organic Field-Effect Transistor. *Adv. Mater.* **2014**, *27*, 911−916.

(48) Debye, P.; Hückel, E. Zur Theorie der Elektrolyte. *Phys. Z.* **1923**, *24*, 185−206.

(49) Cao, C.; Zhang, Y.; Jiang, C.; Qi, M.; Liu, G. Advances on Aryldiazonium Salt Chemistry Based Interfacial Fabrication for Sensing Applications. *ACS Appl. Mater. Interfaces* **2017**, *9*, 5031−5049.

(50) Adali-Kaya, Z.; Tse Sum Bui, B.; Falcimaigne-Cordin, A.; Haupt, K. Molecularly Imprinted Polymer Nanomaterials and Nanocomposites: Atom-Transfer Radical Polymerization with Acidic Monomers. *Angew. Chem., Int. Ed.* **2015**, *54*, 5192−5195.

(51) Van Duin, M.; Peters, J. A.; Kieboom, A. P. G.; Van Bekkum, H. Studies on Borate Esters 1. The Ph Dependence of the Stability of Esters of Boric Acid and Borate in Aqueous Medium as Studied by 11B NMR. *Tetrahedron* **1984**, *40*, 2901−2911.

(52) Lorand, J. P.; Edwards, J. O. Polyol Complexes and Structure of Benzeneboronate Ion. *J. Org. Chem.* **1959**, *24*, 769−774.

(53) Springsteen, G.; Wang, B. A Detailed Examination of Boronic Acid-Diol Complexation. *Tetrahedron* **2002**, *58*, 5291−5300.

(54) Fors, B. P.; Hawker, C. J. Control of a Living Radical Polymerization of Methacrylates by Light. *Angew. Chem., Int. Ed.* **2012**, *51*, 8850−8853.

(55) Kajisa, T.; Sakata, T. Molecularly Imprinted Artificial Biointerface for Enzyme-Free Glucose Transistor. *ACS Appl. Mater. Interfaces* **2018**, *10*, 34983−34990.

(56) Liu, G.; Böcking, T.; Gooding, J. J. Diazonium Salts: Stable Monolayers on Gold Electrodes for Sensing Applications. *J. Electroanal. Chem.* **2007**, *600*, 335−344.

DOI: 10.1021/acsami.8b20010
ACS Appl. Mater. Interfaces 2019, 11, 5561−5569

(57) Taniguchi, I.; Toyosawa, K.; Yamaguchi, H.; Yasukouchi, K. Reversible Electrochemical Reduction and Oxidation of Cytochrome c at a Bis(4-pyridyl) Disulphide-Modified Gold Electrode. *J. Chem. Soc., Chem. Commun.* **1982**, 1032−1033.
(58) Bain, C. D.; Whitesides, G. M. Molecular-Level Control over Surface Order in Self-Assembled Monolayer Films of Thiols on Gold. *Science* **1988**, *240*, 62−63.
(59) Schlenoff, J. B.; Li, M.; Ly, H. Stability and Self-Exchange in Alkanethiol Monolayers. *J. Am. Chem. Soc.* **1995**, *117*, 12528−12536.
(60) Laibinis, P. E.; Whitesides, G. M.; Allara, D. L.; Tao, Y. T.; Parikh, A. N.; Nuzzo, R. G. Comparison of the Structures and Wetting Properties of Self-Assembled Monolayers of N-alkanethiols on the Coinage Metal Surfaces, Copper, Silver, and Gold. *J. Am. Chem. Soc.* **1991**, *113*, 7152−7167.
(61) Chon, S.; Paik, W.-k. Adsorption of Self-Assembling Sulfur Compounds through Electrochemical Reactions: Effects of Potential, Acid and Oxidizing Agents. *Phys. Chem. Chem. Phys.* **2001**, *3*, 3405−3410.
(62) Radi, A.-E.; Muñoz-Berbel, X.; Cortina-Puig, M.; Marty, J.-L. An Electrochemical Immunosensor for Ochratoxin A Based on Immobilization of Antibodies on Diazonium-Functionalized Gold Electrode. *Electrochim. Acta* **2009**, *54*, 2180−2184.
(63) Abel, B. A.; McCormick, C. L. Mechanistic Insights into Temperature-Dependent Trithiocarbonate Chain-End Degradation during the RAFT Polymerization of N -Arylmethacrylamides. *Macromolecules* **2016**, *49*, 465−474.

DOI: 10.1021/acsami.8b20010
ACS Appl. Mater. Interfaces 2019, 11, 5561−5569